

# Subspace Adversarial Training

Tao Li    Yingwen Wu    Sizhe Chen    Kun Fang    Xiaolin Huang\*

Shanghai Jiao Tong University  
 {li.tao, yingwen\_wu, sizhe.chen, fanghenshao, xiaolinhuang}@sjtu.edu.cn

## Abstract

Single-step adversarial training (AT) has received wide attention as it proved to be both efficient and robust. However, a serious problem of catastrophic overfitting exists, i.e., the robust accuracy against projected gradient descent (PGD) attack suddenly drops to 0% during the training. In this paper, we understand this problem from a novel perspective of optimization and firstly reveal the close link between the fast-growing gradient of each sample and overfitting, which can also be applied to understand the robust overfitting phenomenon in multi-step AT. To control the growth of the gradient during the training, we propose a new AT method, subspace adversarial training (Sub-AT), which constrains the AT in a carefully extracted subspace. It successfully resolves both two kinds of overfitting and hence significantly boosts the robustness. In subspace, we also allow single-step AT with larger steps and larger radius, which further improves the robustness performance. As a result, we achieve the state-of-the-art single-step AT performance: our pure single-step AT can reach over 51% robust accuracy against strong PGD-50 attack with radius 8/255 on CIFAR-10, even surpassing the standard multi-step PGD-10 AT with huge computational advantages. The code is released<sup>1</sup>.

## 1. Introduction

Adversarial training (AT) [19], which aims to minimize the model’s risk under the worst-case perturbations, is the currently most effective approach for improving the robustness of deep neural networks. For a given neural network  $f(\mathbf{x}, \mathbf{w})$  with parameters  $\mathbf{w}$ , the optimization objective of AT can be formulated as follows:

$$\min_{\mathbf{w}} \mathbb{E}_{(\mathbf{x}, y) \sim \mathcal{D}} \left[ \max_{\delta \in \mathcal{B}(\mathbf{x}, \epsilon)} \mathcal{L}(f(\mathbf{x} + \delta, \mathbf{w}), y) \right],$$

where  $\mathcal{B}(\mathbf{x}, \epsilon)$  is the norm ball with radius  $\epsilon$  and  $\mathcal{L}$  is the loss function. The key issue of AT lies in solving the inner worst-case problem by generating adversarial examples.

<sup>1</sup><https://github.com/nblt/Sub-AT>

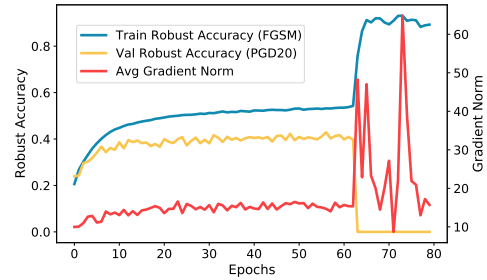


Figure 1. Catastrophic overfitting in single-step AT. The experiments are conducted on CIFAR-10 with PreAct ResNet18 model for adversarial robustness against  $\ell_\infty$  perturbations of radius 8/255. The robust accuracy of single-step Fast AT on the validation set against PGD-20 attack can abruptly drop to 0 in one single epoch, characterized by a rapid explosion of the average gradient norm of each sample.

Presently the most efficient way to generate adversarial examples is the fast gradient sign method (FGSM) [9], i.e.,

$$\mathbf{x}^{\text{adv}} = \mathbf{x} + \epsilon \cdot \text{sgn}(\nabla_{\mathbf{x}} \mathcal{L}(f(\mathbf{x}, \mathbf{w}), y)).$$

Since the adversarial examples above are generated by one-step gradient propagation, the corresponding AT is called *single-step* AT. In Fig. 1, we demonstrate a standard single-step AT process where the robust accuracy on the training set against FGSM attack keeps increasing. However, the generalization capability, i.e., the robust accuracy on the validation set under projected gradient descent (PGD) attack [19], can suddenly drop to zero, which is a typical overfitting phenomenon referred as *catastrophic overfitting* [30].

Many works [1, 14, 30] are devoted to resolving such an intriguing overfitting problem. One approach to tackle the overfitting is to use a judiciously designed learning rate schedule as well as appropriate regularizations. For example, Wong *et al.* [30] proposed to add a random step to FGSM and introduce cyclic learning rates to overcome the overfitting. Andriushchenko *et al.* [1] proposed a novel regularization term called GradAlign to further improve the quality of the single-step AT solution. However, these methods highly rely on a proper learning rate schedule, and

they need to tune it carefully when it comes to different tasks. Overfitting can happen when applying other commonly used schedules, such as piecewise learning rates. Another approach is to generate more precise adversarial examples. For example, Kim *et al.* [14] suggested verifying the inner interval along the adversarial direction and searching for appropriate step size. PGD AT, a typical *multi-step* AT which generates the adversarial examples using multiple iterations, can also help avoid catastrophic overfitting. However, these methods require multiple forward propagations, and more seriously, overfitting can still prominently occur in the multi-step AT (known as *robust overfitting*) as demonstrated by Rice *et al.* [23].

In order to have an in-depth understanding of this phenomenon, let us investigate what happens at the 64-th epoch in Fig. 1 when catastrophic overfitting occurs. Before that time, the training robust accuracy has already stepped into a stable stage, indicating that the norm of the batch gradient  $\|\frac{1}{n} \sum_{i=1}^n \nabla_{\mathbf{w}} \mathcal{L}(f(\mathbf{x}_i^{\text{adv}}, \mathbf{w}), y)\|$  is small ( $n$  denotes the batch size). There are two possibilities for the small average gradient norm: *i*) the gradient of each sample is small; *ii*) the gradient of each sample does not converge, but they cancel each other, resulting in an overall balanced state. In Fig. 1, we plot the average gradient norm of each sample in a fixed training batch, i.e.,  $\frac{1}{n} \sum_{i=1}^n \|\nabla_{\mathbf{w}} \mathcal{L}(f(\mathbf{x}_i^{\text{adv}}, \mathbf{w}), y)\|$  in red. An interesting observation is that the average norm of the gradient abruptly increases at the moment catastrophic overfitting happens. Intuitively, at that time, the neural network tries to capture each sample’s label with huge fluctuations, namely, large gradients, which is a significant signal of overfitting. This phenomenon also coincides with the recent discussion on the connection between the gradient variance and generalization capability [13].

There is a close link between the large gradients and overfitting, which will be discussed in detail in Sec. 3.1. Inspired by this link, we propose to control the magnitude of the gradient to resolve the overfitting. One straightforward way is to add a regularization term on the gradient norm. However, it would bring considerable additional computational overheads as it requires second-order derivatives, and even worse, it may harm the neural networks’ approximation capability [3, 8]. Another possible way is to restrict the gradient descent in a subspace instead of the whole parameter space to prevent the excessive growth of the gradient. The key challenge lies in keeping the neural network’s capability in such a subspace, which has been recently discussed in [17] showing that optimizing the parameters in a tiny subspace extracted from training dynamics could keep the neural network’s performance. Based on this discovery, we propose a new AT method called *Subspace Adversarial Training (Sub-AT)*, which first identifies such an effective subspace and then conducts AT on it. From the training statistics of Sub-AT in Fig. 2a, we can find that it success-

fully controls the average gradient norm under a constant low level (the yellow dotted curve), thus resolving the catastrophic overfitting. Meanwhile, it significantly improves the robust accuracy from 0.4 to nearly 0.5 (the yellow solid curve). The sensitivity to learning rates is also fundamentally overcome as we only use a constant learning rate and can obtain similar results across a wide range of learning rates. As a direct extension, Sub-AT can be applied to multi-step AT to mitigate the robust overfitting (Fig. 2b), implying that the two different phenomena share similar essence. Thus for the first time, the two overfitting phenomena previously considered to be treated separately [1] are now connected and resolved in a unified approach.

Since training in subspace can control the magnitude of the gradient and thus fundamentally resolve the catastrophic overfitting, we now can allow using larger steps and larger radius, which were previously considered as two major obstacles in single-step AT [1, 30]. Via Sub-AT, we not only successfully overcome these two obstacles but also further improve the robustness performance. As a result, pure single-step-based AT for the first time achieves comparable or even better robustness than standard multi-step PGD-10 AT against strong PGD-50 attack with a huge computational superiority, answering the long-existing question:

*Can single-step AT achieve comparable robustness against iterative attack than multi-step AT?*

Thus our new AT method uncovers the long-neglected potential of single-step AT and can enlighten more efficient and powerful AT algorithms.

Our main contributions can be summarized as follows:

- We understand the *catastrophic overfitting* in single-step AT from a novel view of optimization that reveals the close link between the abrupt increase of average gradient norm and overfitting. It can also be applied to understand the *robust overfitting* in multi-step AT.
- We propose an efficient AT method, Sub-AT, which constrains the AT in a carefully extracted subspace to control the fast growth of the gradient. It resolves both two kinds of overfitting in AT uniformly and then significantly improves the robustness.
- Our Sub-AT achieves the *state-of-the-art* adversarial robustness on single-step AT and can also successfully train with larger steps and larger radius, which brings further improvements. Notably, our pure single-step AT achieves over 51% robust accuracy against PGD-50 attack with  $\epsilon = 8/255$  on CIFAR-10, outperforming the multi-step PGD-10 AT with great time benefits.

## 2. Related Work

**Adversarial Training.** Since deep neural networks are easily fooled by adversarial examples, many defense meth-

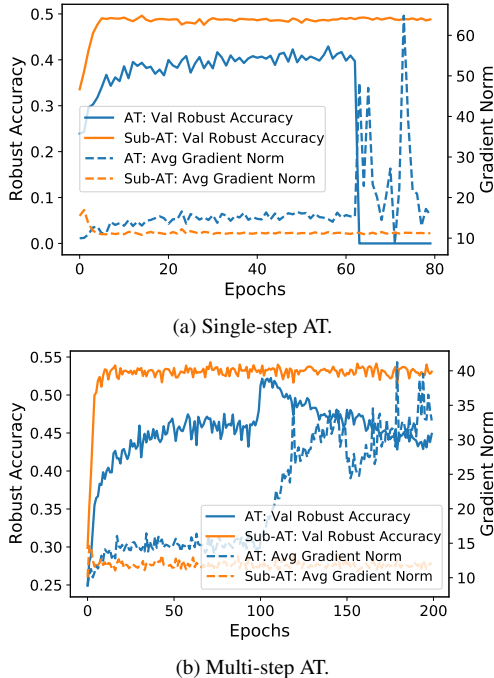


Figure 2. Resolving *catastrophic overfitting* in single-step AT and *robust overfitting* in multi-step AT. The experiments are conducted on CIFAR-10 with PreAct ResNet18 model for robustness against  $\ell_\infty$  perturbations of radius  $8/255$ . In both overfittings, robust accuracy on the validation set degenerates along with an abrupt increase of the average grad norm of the sample. Our Sub-AT can successfully control the rapid increase of the average grad norm, thereby resolving both two overfittings uniformly and significantly improving the robustness.

ods [5, 18–20, 22, 25, 28, 29, 32, 33] have been proposed. Among them, AT [19], which augments the training data with adversarial perturbations, is currently the most effective way to improve the robustness of the model. According to the times of gradient propagation involved in generating adversarial perturbations, AT can be mainly divided into two classes: single-step AT [1, 14, 24, 30] and multi-step AT [19, 28, 33]. Single-step AT has proven to be both efficient and robust [24, 30] and thus receives much attention. For example, Free AT [24] achieves remarkable robustness performance using a single-step gradient with redundant batches and accumulative perturbations. Multi-step AT, such as PGD AT [19] and TRADES [33], generally provides better robustness guarantees than single-step AT as it generates strong adversarial perturbations. However, its computational cost is relatively high as multiple forward and back propagations are required during batch training.

**Overfitting in Adversarial Training.** Both single-step AT and multi-step AT suffer from overfitting problems (known as catastrophic overfitting [30] and robust overfit-

ting [23], respectively) where the robust test accuracy suddenly begins to decrease as the training proceeds. The problem can be more severe in single-step AT as the robust test accuracy against PGD attack can abruptly drop to 0% only in one epoch. Many works are devoted to resolving such an intriguing overfitting problem. Among them, Wong *et al.* [30] first suggested adding a random step to FGSM and adopting cyclic learning rates, which provides competitive robustness against PGD AT with significant time advantages. Andriushchenko *et al.* [1] designed a novel regularization term called GradAlign to improve the gradient alignment inside the perturbation set and provide better robustness. However, these methods rely on a judiciously selected learning rate schedule, or a proper regularization coefficient [14]. Towards understanding the overfitting, Vivek *et al.* [27] discovered that models trained via single-step AT learn to prevent the model from generating effective adversarial examples and introduced dropout scheduling to mitigate it. Kim *et al.* [14] observed the distortion of the sample-wise decision boundary during the overfitting and suggested verifying the adversarial examples along the adversarial direction. However, their explanations are limited to single-step AT, and the robustness performance is still inferior. In this work, we understand overfitting from a general perspective of optimization and explain both kinds of overfitting in AT uniformly, bringing a huge improvement in robustness.

**Training in Subspace.** Many works focus on the low-dimensionality essence of neural network training [11, 26]. The pioneering work [16] first proposed to train neural networks in a reduced subspace via random projection and discovered that the required dimension to obtain 90% performance of regular training is far less than the original parameters’ dimension. The following work [10] improved random projection performance by considering different layers and re-drawing the random bases at each step. Different from random projection, Li *et al.* [17] proposed to train neural networks in low-dimensional subspaces extracted from training dynamics and obtained comparable performance as regular training. We also take advantage of the subspace extracted from the training dynamics of AT and constrain the training in it, thereby successfully controlling the magnitude of the gradient and keeping the training performance.

### 3. Methodology

#### 3.1. Investigating Catastrophic Overfitting

We first focus on the interesting phenomenon in Fig. 3a: when catastrophic overfitting occurs, the natural accuracy on the training data also goes through a collapse. Recall that at the same time, the robust training accuracy goes through a sudden increase, as illustrated in Fig. 1. These two phenom-

ena suggest that before the overfitting, the network learns robust features that benefit both robust accuracy and natural accuracy. However, when overfitting occurs, the network tries to capture the adversarial information in training data (with adversarial perturbations), which harms the natural accuracy, i.e., the generalization capability to natural examples. Further, it loses the generalization capability to new adversarial examples generated by PGD attack as they may lie in a small ball around the natural examples. The adversarial information is so “hard” to learn that the network has to go through a huge fluctuation and finally overfit it, resulting in zero robust accuracy on test data.

Since adversarial examples are relatively “hard” to learn, we then pay attention to the evolution of each sample’s gradient and consider the average norm of the gradient to analyze the training state. Specifically, we record the robust accuracy of Fast AT [30] against PGD-20 attack and the average norm of the gradient in one fixed training batch with size  $n = 256$  during the training (the estimations for batch normalization are frozen for sample-wise gradient estimation). Fig. 1 illustrates the statistics when the catastrophic overfitting occurs, where we can find that the abrupt decrease of the robust accuracy highly coincides with the sudden increase of the average gradient norm. This phenomenon implies that during the catastrophic overfitting, the gradient of each sample suddenly increases, resulting in a huge fluctuation in training and, finally, significant degeneration of the robust generalization.

To further investigate the link between increasing gradients and overfitting, we examine the detailed statistics in the 64th epoch when catastrophic overfitting happens. We record the statistics after every iteration. For comparison, we also consider decaying the learning rate in advance from 0.1 to 0.01 before the epoch training as increasing gradient indicates an excessive learning rate. The results are illustrated in Fig. 3b, where we can find that although for both learning rates catastrophic overfitting eventually occurs, using a smaller learning rate could help. It achieves better robustness accuracy and remarkably postpones the overfitting with a better controlled average gradient norm (the yellow dotted curve). We summarize our findings as follows: *i*) the overfitting is closely related to the fast-growing of the average gradient norm, and a delicately chosen learning rate could help suppress the growth of the gradient, which results in recent advances on adopting cyclic learning rates [30]; *ii*) to control the catastrophic overfitting, we have to control the growth of the average gradient norm.

### 3.2. Controlling the Gradient Magnitude

Let us focus on how to control the gradient magnitude of each sample during the training. Our main idea is to constrain the gradient descent of AT in a low-dimensional subspace instead of the whole parameter space, thus implicitly

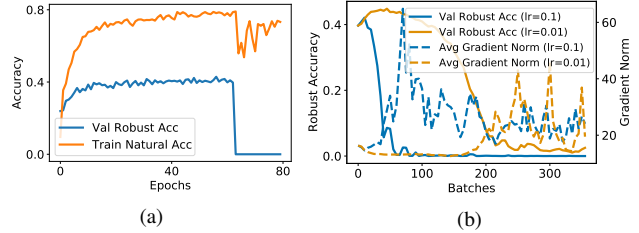


Figure 3. (a) natural accuracy on training data also collapses at the overfitting; (b) the variation of the statistics in the 64th epoch: switching to a smaller learning rate could alleviate the catastrophic overfitting with a better-controlled gradient norm.

suppressing the fast growth of the gradient. First, we consider how to obtain such a subspace that is effective for AT. Recently, Li *et al.* [17] proposed an algorithm called DLDR, which can effectively extract a low-dimensional subspace for optimization from the training trajectory. It generally contains two stages:

1. Sample a few model checkpoints  $\{\mathbf{w}_1, \mathbf{w}_2, \dots, \mathbf{w}_t\}$  during the regular training where we align the model parameters as a vector  $\mathbf{w}_i$  with length of the parameters’ number  $N$ ;
2. Perform singular vector decomposition on the aligned parameter matrix  $[\mathbf{w}_1, \mathbf{w}_2, \dots, \mathbf{w}_t]$  to obtain the mutually orthogonal bases of the subspace  $[\mathbf{u}_1, \mathbf{u}_2, \dots, \mathbf{u}_d]$ , where  $d$  is the dimensionality of the subspace.

In this work, we apply the DLDR algorithm [17] to extract the effective subspace of AT. Note that we sample the model parameters before the overfitting occurs since in this period, the network learns robust features benefiting both robust accuracy and natural accuracy as demonstrated in Sec. 3.1. We expect that optimizing the neural network in such extracted subspace could overcome the overfitting and obtain good robustness. After extracting the effective subspace for AT, we rewind the model to the parameter initialization and constrain the optimization in the obtained subspace by projecting the gradient on it. The detailed algorithm is summarized in Algorithm 1.

**Sampling Strategy:** In this work, we by default adopt a simple strategy: sampling twice uniformly in each epoch training. A more delicate strategy could improve the performance. However, it is not the main focus of this work. The dimensionality of the subspace  $d$  is set to 80 on CIFAR-10 for single-step AT by default. We provide a detailed sampling strategy in Appendix A.

**Training Performance:** In Fig. 2, we demonstrate that Sub-AT can successfully control the average gradient norm under a constant low level, thereby resolving both catastrophic overfitting and robust overfitting meanwhile significantly improving the robustness performance. Then in

---

**Algorithm 1** Subspace Adversarial Training (Sub-AT)

**Require:** The dimensionality of the subspace  $d$ , the number of sampling times  $t$  for DLDR, learning rate  $\alpha$ , batch size  $n$  and training data  $\{(\mathbf{x}_i, y_i)\}$ ;

- 1: // DLDR stage for obtaining the orthonormal bases  $[\mathbf{u}_1, \mathbf{u}_2, \dots, \mathbf{u}_d]$  of the desired subspace;
- 2: Sample a parameter trajectory  $\{\mathbf{w}_1^s, \mathbf{w}_2^s, \dots, \mathbf{w}_t^s\}$  along the standard AT training according to certain strategy;
- 3:  $\bar{\mathbf{w}} = \frac{1}{t} \sum_{i=1}^t \mathbf{w}_i^s$ ;
- 4:  $W = [\mathbf{w}_1^s - \bar{\mathbf{w}}, \mathbf{w}_2^s - \bar{\mathbf{w}}, \dots, \mathbf{w}_t^s - \bar{\mathbf{w}}]$ ;
- 5: Perform spectral decomposition on  $W^\top W$  and obtain the largest  $d$  eigenvalues  $[\sigma_1^2, \sigma_2^2, \dots, \sigma_d^2]$  with the corresponding eigenvectors  $[\mathbf{v}_1, \mathbf{v}_2, \dots, \mathbf{v}_d]$ ;
- 6:  $\mathbf{u}_i = \frac{1}{\sigma_i} W \mathbf{v}_i$ ;
- 7: // Sub-AT stage for performing AT in subspace;
- 8: Initialize  $k \leftarrow 0$ ;
- 9:  $P = [\mathbf{u}_1, \mathbf{u}_2, \dots, \mathbf{u}_d]$ ;
- 10:  $\mathbf{w}_0 = \mathbf{w}_1^s$ ;  $\triangleright$  Rewind the parameters to initialization
- 11: **while** not converging **do**
- 12:   Sample the mini-batch data  $\{(\mathbf{x}_i, y)\}_{i=1}^n$ ;
- 13:   Compute the adversarial examples  $\{\mathbf{x}_i^{\text{adv}}\}_{i=1}^n$ ;
- 14:    $\mathbf{g}_k^{\text{adv}} \leftarrow \frac{1}{n} \sum_{i=1}^n \nabla_{\mathbf{w}} \mathcal{L}(f(\mathbf{x}_i^{\text{adv}}, \mathbf{w}_k), y)$ ;
- 15:    $\mathbf{w}_{k+1} \leftarrow \mathbf{w}_k - \alpha P (P^\top \mathbf{g}_k^{\text{adv}})$ ;
- 16:    $k \leftarrow k + 1$ ;
- 17: **end while**
- 18: Return  $\mathbf{w}_k$ ;

---

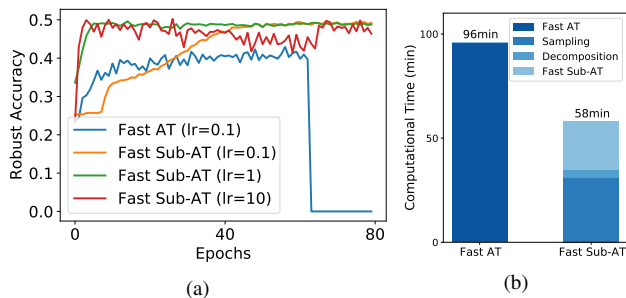


Figure 4. (a) Sub-AT is extremely robust to learning rate; (b) detailed time consumption analysis on CIFAR-10.

Fig. 4a, we demonstrate that Sub-AT is also highly robust to a wide range of learning rates and can converge even with only a constant learning rate. Notably, with a large learning rate, Sub-AT can converge in a few epochs and keep the performance without catastrophic overfitting. Thus our Sub-AT fundamentally overcomes the sensitivity to learning rates and obtains true robustness to overfitting. In this work, we set the learning rate as 1 by default for both stable and efficient training.

**Computational Analysis:** The computational overhead of Sub-AT consists of two parts: DLDR and training in subspace. The DLDR part contains two stages: sampling and

decomposition. The time consumption on the decomposition can be negligible compared to the sampling as it only involves a spectral decomposition of a  $t \times t$  matrix and two matrix productions. The training of Sub-AT has almost the same computational complexity as the standard AT with little additional cost on the gradient projection. Detailed time consumption analysis on CIFAR-10 is illustrated in Fig. 4b. We can find that our Sub-AT reduces the total training time overhead compared to standard AT training as it only requires sampling a small piece of the trajectory with very efficient training in the subspace.

## 4. Experiments

In this section, we conduct comprehensive experiments to verify the effectiveness of Sub-AT in resolving the overfitting of both single-step AT and multi-step AT. We first demonstrate that our Sub-AT can successfully resolve the catastrophic overfitting and achieve the *state-of-the-art* robustness performance in single-step AT. Then we show that after obtaining the subspace, Sub-AT can allow training with larger steps and larger radius, which further improves the robustness and obtains a comparable robustness performance against multi-step AT with significant computational advantages. Finally, we apply Sub-AT to mitigate the robust overfitting in multi-step AT and show that leveraging the subspace, weak single-step AT can achieve even better robustness than multi-step AT, revealing the underestimated potential of single-step AT.

### 4.1. Experiments Setup

**Datasets:** Three datasets are considered in our experiments: CIFAR-10, CIFAR-100 [15] and Tiny-ImageNet [7]. In all experiments, we randomly split the original training set as training and validation according to a ratio of 9:1 [4]. Due to the limited space, we place the Tiny-ImageNet results in Appendix C.

**Attack Methods:** We consider two typical types of perturbations:  $\ell_\infty$  norm with radius  $\epsilon = 8/255$  and  $\ell_2$  norm with radius  $\epsilon = 128/255$ . For single-step AT, we focus on  $\ell_\infty$  norm attack and use the recommended step size of  $\alpha = 1.25\epsilon$  described by Wong *et al.* [30]. For multi-step AT, by default we generate adversarial perturbations with 10 steps attacks with step size  $\alpha = 2/255$  for  $\ell_\infty$  norm and  $\alpha = 15/255$  for  $\ell_2$  norm following the setting of Rice *et al.* [23]. For robustness evaluation, we consider PGD-20 [23], PGD-50 (with 50 iterations and 10 restarts) [30] and Auto-Attack, a strong and reliable attack recently proposed by [6], for a rigorous evaluation.

**Training:** For all experiments, we by default use Pre-Act ResNet-18 [12] model. Experiments with Wide-ResNet [31] can be found in Appendix D. Three learning rate schedules are considered: *i) cyclic* schedule [1,30] which can help overcome overfitting; *ii) piecewise* schedule, i.e., training

Table 1. Performance comparisons of single-step AT on CIFAR-10/100. The robustness is evaluated under **PGD-50** attack.

| Schedule  | Method           | Subspace  | CIFAR-10        |              |                  |       | CIFAR-100       |              |                  |       |
|-----------|------------------|-----------|-----------------|--------------|------------------|-------|-----------------|--------------|------------------|-------|
|           |                  |           | Robust Accuracy |              | Natural Accuracy |       | Robust Accuracy |              | Natural Accuracy |       |
|           |                  |           | Best            | Final        | Best             | Final | Best            | Final        | Best             | Final |
| cyclic    | Fast AT          | –         | 45.82           | 45.69        | 82.36            | 83.26 | 16.72           | 0.00         | 34.51            | 47.23 |
| cyclic    | GradAlign        | –         | 47.02           | 46.73        | 80.43            | 81.34 | 24.57           | 24.22        | 50.82            | 51.92 |
| piecewise | Fast AT          | –         | 39.95           | 0.00         | 73.13            | 89.93 | 17.84           | 0.00         | 41.54            | 46.46 |
| piecewise | Single AT        | –         | 35.48           | 32.43        | 83.68            | 86.86 | 16.18           | 0.91         | 55.88            | 59.15 |
| piecewise | Free AT          | –         | 47.30           | 47.00        | 79.37            | 79.98 | 23.50           | 22.93        | 50.91            | 51.64 |
| piecewise | GradAlign        | –         | 42.16           | 0.02         | 71.64            | 88.77 | 23.80           | 15.60        | 49.30            | 53.40 |
| constant  | Fast Sub-AT      | Fast AT   | 48.22           | 47.88        | 82.36            | 82.74 | 24.97           | 24.55        | 52.74            | 53.09 |
| constant  | GradAlign Sub-AT | GradAlign | <b>48.88</b>    | <b>48.40</b> | 79.82            | 80.84 | <b>25.69</b>    | <b>25.46</b> | 52.65            | 52.92 |

Table 2. Results of single-step Sub-AT with a larger training  $\epsilon$  against  $\ell_\infty$  perturbations of radius  $8/255$  on CIFAR-10 ( $\alpha = 1.25\epsilon$ ).

| Method                              | Subspace | Best    |              |              | Final   |              |              | Time |
|-------------------------------------|----------|---------|--------------|--------------|---------|--------------|--------------|------|
|                                     |          | Natural | PGD-50       | AA           | Natural | PGD-50       | AA           |      |
| Fast AT                             | –        | 73.13   | 39.95        | 37.55        | 89.93   | 0.00         | 0.00         | 1.6h |
| Fast Sub-AT ( $\epsilon = 8/255$ )  | Fast AT  | 82.36   | 48.22        | 44.20        | 82.74   | 47.88        | 43.89        | 1.0h |
| Fast Sub-AT ( $\epsilon = 12/255$ ) | Fast AT  | 80.74   | 50.38        | 45.84        | 80.91   | 49.64        | 45.40        | 1.0h |
| Fast Sub-AT ( $\epsilon = 16/255$ ) | Fast AT  | 77.34   | <b>51.46</b> | <b>45.92</b> | 77.88   | <b>51.22</b> | <b>45.70</b> | 1.0h |
| PGD-10 AT                           | –        | 80.50   | 50.79        | 47.29        | 82.92   | 42.51        | 41.08        | 7.0h |

the model for 200 epochs with an initial learning rate of 0.1 and decaying the learning rate by ten at 100 and 150 epochs (as our default setting for baseline AT), which is commonly used and produces the best robustness performance as suggested by Rice *et al.* [23]; *iii*) *constant* schedule, which is adopted for our Sub-AT to show its insensitivity to the learning rate. We set the learning rate as 1 *without* a schedule and train the model for 40 epochs in subspace with a sufficient convergence. Data augmentations, such as 4-pixel padding, random cropping, and horizontal flipping, are applied.

**Evaluation:** We both consider the best and the final robustness performance and use the difference between them to evaluate the degree of overfitting. The model checkpoint that achieves the best robust accuracy on the validation set is selected as the best model during the training, while the final is an average of the last five epochs [23] (except that cyclic learning rates use the last epoch). The time consumption is measured on an Nvidia Geforce GTX 2080 TI. For Sub-AT, we repeat over five independent runs. The standard deviations in tables are omitted as they are very small ( $\leq 0.45\%$ ), which hardly affects the results.

## 4.2. Resolving Catastrophic Overfitting

First, we consider resolving the catastrophic overfitting in single-step AT. We set the Fast AT [30], i.e., FGSM AT with a random initialization, as the baseline, and also consider other recently proposed methods for preventing the

overfitting, including GradAlign (with a recommended coefficient  $\lambda = 0.2$ ) [1], Stable Single-AT (with  $c = 3$  check points) [14] and Free AT ( $m = 8$ ) [24]. We evaluate the adversarial robustness using strong PGD-50 attack following [30]. For examining whether catastrophic overfitting occurs, the number of total training epochs is set to 200 [14].

The results of different methods on both CIFAR-10 and CIFAR-100 datasets are presented in Tab. 1, where our Sub-AT is conducted in the subspace extracted from the training trajectory of AT with a piecewise learning rate schedule (e.g., Fast Sub-AT is training in the subspace extracted from Fast AT with a piecewise schedule). We can find that under the piecewise learning rate schedule, previous Fast AT and FGSM AT with a GradAlign regularization can still meet catastrophic overfitting. A carefully designed cyclic learning rate schedule [1, 30] can help the model overcome the overfitting, however, it leads to an inferior robust performance (e.g.,  $-1.86\%$  on CIFAR-10) compared with our GradAlign Sub-AT. Without any other regularization technique, our naive Fast AT in subspace is already able to obtain better robustness than previously best single-step AT performance with GradAlign regularization [1]. To further ensure the improved robustness, we additionally evaluate the robust accuracy via Auto-Attack. On CIFAR-10, our best GradAlign Sub-AT achieves  $44.89 \pm 0.31\%$  robust accuracy while best cyclic GradAlign achieves  $43.25 \pm 0.23\%$ , and on CIFAR-100, our

best GradAlign Sub-AT achieves  $21.64 \pm 0.22\%$  while best cyclic GradAlign achieves  $20.30 \pm 0.11\%$ . Thus via Sub-AT, we obtain the *state-of-the-art* robustness performance on the single-step AT, which further shortens the robustness gap between single-step AT and multi-step AT. Note that our good performance does not rely on the results obtained during the DLDR sampling, as both vanilla Fast AT and GradAlign meet serious overfitting during the training and only obtain a poor result far from satisfactory.

### 4.3. Towards Larger Steps and Larger Radius

After resolving the catastrophic overfitting, we demonstrate that our Sub-AT can overcome the overfittings in training with a large step and a large radius, two major obstacles in single-step AT, which further improves the robustness performance.

**Single-step AT with a larger step.** Although Wong *et al.* [30] discovered that adding a random initialization to FGSM AT could help avoid catastrophic overfitting, it only holds if the selected step size  $\alpha$  is not too large. In fact, applying  $\alpha$  larger than  $12/255$  could still meet serious catastrophic overfitting (as illustrated in Fig. 3 of [30] for  $\epsilon = 8/255$ ). Since our Sub-AT can resolve the catastrophic overfitting, we expect it can successfully train with a large  $\alpha$ . Specifically, we focus on CIFAR-10 and repeat the Fast Sub-AT experiments in Sec. 4.2 with  $\alpha$  ranging from  $1/255$  to  $16/255$  and record the final robustness performance (note that we are in the same subspace). From the results in Fig. 5, we can find that after successfully resolving the overfitting for a large step size, our Sub-AT can further continuously improve the robustness, showing that using a larger step could indeed benefit robustness.

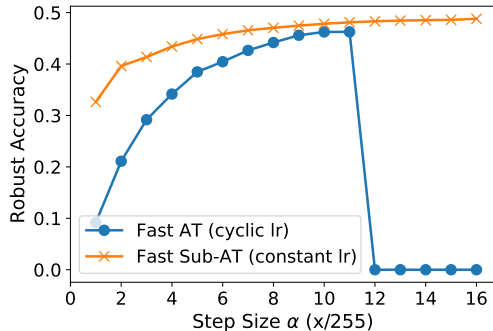


Figure 5. **Final** robust test accuracy of different single-step methods under PGD-20 attack over different step sizes for  $\epsilon = 8/255$ .

**Single-step AT with a larger radius.** AT with a larger radius  $\epsilon$  generally could provide better robustness guarantees against potential adversarial attacks. However, it is hard to train a model that is robust to a large  $\epsilon$ , especially for single-step AT [1]. By constraining the training in subspace, we can now conduct single-step AT with a large  $\epsilon$

with ease. Similar to the last section, we repeat the Fast Sub-AT experiments in Sec. 4.2 with training  $\epsilon$  ranging from  $8/255$  to  $20/255$  ( $\alpha = 1.25\epsilon$ ). We select the best model checkpoint against PGD-20 attack with  $\epsilon = 8/255$  and plot the test robust accuracy curves of different settings against PGD-20 attack with  $\epsilon$  ranging from  $8/255$  to  $16/255$  in Fig. 6. We can find that training with a larger radius within a proper range could consistently improve the model robustness against attacks of different radius, especially for the large radius attacks. This result implies that after applying larger training  $\epsilon$ , the robustness of the model is genuinely improved. However, there also exist limitations as expected since excessive perturbations will harm the valuable information of training data, resulting in a degenerated performance. For example, we achieve the best robustness against  $8/255$  attack with a training radius  $16/255$ .

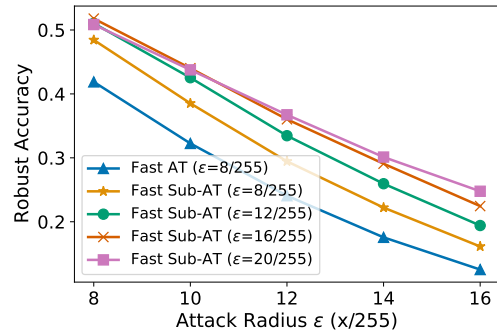


Figure 6. Test robust accuracy under PGD-20 attack with respect to different perturbation radius. We evaluate the checkpoint with the best performance on the validation set.

We summarize our key results of training with larger steps and larger radius in Tab. 2, where we also consider total training time consumption as well as evaluations on PGD-50 and Auto-Attack. The main findings include: *i*) by simply increasing the step size and radius, our Sub-AT can significantly improve the model robustness against the two strong attacks without the problem of catastrophic overfitting; *ii*) notably, our single-step-based Sub-AT can achieve a very competitive robust accuracy under Auto-Attack and even better robust accuracy under PGD-50 attack than multi-step PGD-10 AT. We also get rid of the serious problem of robust overfitting, which PGD-10 AT suffers. *iii*) more promisingly, our Sub-AT only takes a seventh of the training time consumption compared with PGD-10 AT, which is a considerable superiority.

### 4.4. Extensions to Multi-step AT

We then apply Sub-AT to multi-step AT. First, we focus on mitigating robust overfitting and set standard PGD-10 AT [19] as the baseline. To numerically show the degree of the overfitting, we report the difference between best robust

Table 3. Results of multi-step AT and Sub-AT on CIFAR-10/100 against **PGD-20** attack with  $\ell_2$  and  $\ell_\infty$  norm perturbations.

| Dataset   | Norm          | Radius                       | Settings | Robust Accuracy |              |             | Natural Accuracy |       |       |
|-----------|---------------|------------------------------|----------|-----------------|--------------|-------------|------------------|-------|-------|
|           |               |                              |          | Best            | Final        | Diff.       | Best             | Final | Diff. |
| CIFAR-10  | $\ell_\infty$ | $\epsilon = \frac{8}{255}$   | AT       | 51.09           | 42.92        | 8.17        | 80.50            | 82.92 | -2.42 |
|           |               |                              | Sub-AT   | <b>52.79</b>    | <b>52.31</b> | <b>0.48</b> | 80.46            | 80.47 | -0.01 |
|           | $\ell_2$      | $\epsilon = \frac{128}{255}$ | AT       | 67.73           | 65.21        | 2.52        | 88.17            | 88.82 | -2.42 |
|           |               |                              | Sub-AT   | <b>69.14</b>    | <b>69.01</b> | <b>0.13</b> | 88.87            | 88.84 | -0.01 |
| CIFAR-100 | $\ell_\infty$ | $\epsilon = \frac{8}{255}$   | AT       | 26.80           | 19.38        | 7.42        | 52.29            | 53.27 | -0.98 |
|           |               |                              | Sub-AT   | <b>27.50</b>    | <b>27.02</b> | <b>0.48</b> | 52.41            | 52.18 | 0.23  |
|           | $\ell_2$      | $\epsilon = \frac{128}{255}$ | AT       | 40.21           | 34.98        | 5.23        | 61.98            | 60.28 | 1.70  |
|           |               |                              | Sub-AT   | <b>41.48</b>    | <b>41.00</b> | <b>0.48</b> | 62.62            | 63.13 | -0.51 |

Table 4. Results of extending single-step Sub-AT with a larger training  $\epsilon$  to multi-step AT’s subspace against  $\ell_\infty$  perturbations of radius  $8/255$  on CIFAR-10.

| Method                              | Subspace  | Best    |              |              | Final   |              |              | Time |
|-------------------------------------|-----------|---------|--------------|--------------|---------|--------------|--------------|------|
|                                     |           | Natural | PGD-50       | AA           | Natural | PGD-50       | AA           |      |
| PGD-10 AT                           | –         | 80.50   | 50.79        | 47.29        | 82.92   | 42.51        | 41.08        | 7.0h |
| PGD-10 Sub-AT                       | PGD-10 AT | 80.46   | 52.48        | 48.37        | 80.47   | 52.01        | 47.88        | 4.9h |
| Fast Sub-AT ( $\epsilon = 12/255$ ) | PGD-10 AT | 81.02   | 53.32        | 48.58        | 81.25   | 52.85        | 48.21        | 3.9h |
| Fast Sub-AT ( $\epsilon = 16/255$ ) | PGD-10 AT | 79.63   | <b>54.17</b> | <b>49.14</b> | 79.94   | <b>54.11</b> | <b>48.86</b> | 3.9h |

accuracy (when early stopping during the training) and final robust accuracy. The difference is crucial as, generally, we can only obtain the final performance without using the validation set. From the results in Tab. 3, we can find that robust overfitting occurs in every setting of AT as expected, and the robust accuracy gap between the best and the final can be as large as 8.17% (on CIFAR-10 with  $\ell_\infty$  norm). By restricting the AT in subspace, our Sub-AT can reduce the gap to less than 0.5% meanwhile significantly boosting the robust accuracy (e.g., +1.7% on CIFAR-10). Thanks to the good subspace obtained by DLDR algorithm [17], the generalization on the clean data is also kept compared with standard AT. More examinations on the improvement of the robustness via Auto-Attack are presented in Appendix B. We can find that our Sub-AT can mitigate the robust overfitting and consistently improve the model robustness, demonstrating that training in subspace can genuinely overcome the overfitting and improve the model robustness rather than as a result of gradient masking [2, 21]. It is worth noting that our robustness improvements naturally benefit from the low-dimensional optimization, and the results are promising to be further improved via combining other enhancement techniques, such as modifications on the loss function [4].

Finally, we apply single-step Fast Sub-AT in the subspace extracted from multi-step PGD-10 AT. From the results in Tab. 4, we can find that, surprisingly, Fast Sub-AT with a larger radius can even achieve significantly better robust accuracy than multi-step PGD-10 Sub-AT. It implies

that we can achieve strong robustness only with the guidance of weak adversarial examples in the subspace, which also brings great computational benefits. This encouraging finding reveals the previously underestimated potential of single-step AT and provides a new scheme for designing more robust and efficient AT methods.

## 5. Conclusion

In this paper, we focus on the serious catastrophic overfitting phenomenon in the efficient single-step AT. From the novel perspective of optimization, we reveal the close link between the fast-growing gradient of each sample and overfitting, which can also explain the robust overfitting in multi-step AT. To control the growth of the gradient, Sub-AT is proposed to constrain the AT in a carefully extracted subspace. It successfully resolves both two kinds of overfitting in AT uniformly and hence significantly improves the robustness. Leveraging the subspace, we allow single-step AT with larger steps and a larger radius, which further improves the robustness. Weak adversarial examples generated from single-step AT can be trained to obtain even better robustness than those from multi-step PGD AT in subspace, revealing the great potential of single-step AT. As a result, our pure single-step-based AT can achieve even better robustness than standard PGD-10 AT against the strong PGD-50 attack with only one-seventh of the training time, which is a solid step towards more efficient AT methods.

## References

- [1] Maksym Andriushchenko and Nicolas Flammarion. Understanding and improving fast adversarial training. In *Proceedings of the Advances In Neural Information Processing Systems 33 (NeurIPS)*, volume 33, pages 16048–16059, 2020. [1](#), [2](#), [3](#), [5](#), [6](#), [7](#)
- [2] Anish Athalye, Nicholas Carlini, and David Wagner. Obfuscated gradients give a false sense of security: Circumventing defenses to adversarial examples. In *International Conference on Machine Learning (ICML)*, pages 274–283. PMLR, 2018. [8](#), [11](#)
- [3] David GT Barrett and Benoit Dherin. Implicit gradient regularization. In *International Conference on Learning Representations (ICLR)*, 2020. [2](#)
- [4] Tianlong Chen, Zhenyu Zhang, Sijia Liu, Shiyu Chang, and Zhangyang Wang. Robust overfitting may be mitigated by properly learned smoothing. In *International Conference on Learning Representations (ICLR)*, 2020. [5](#), [8](#), [11](#)
- [5] Francesco Croce, Maksym Andriushchenko, Vikash Sehrawag, Nicolas Flammarion, Mung Chiang, Prateek Mittal, and Matthias Hein. Robustbench: a standardized adversarial robustness benchmark. In *Advances in Neural Information Processing Systems (NeurIPS) Datasets and Benchmarks Track (Round 2)*, 2020. [3](#)
- [6] Francesco Croce and Matthias Hein. Reliable evaluation of adversarial robustness with an ensemble of diverse parameter-free attacks. In *International Conference on Machine Learning (ICML)*, pages 2206–2216. PMLR, 2020. [5](#), [11](#)
- [7] Jia Deng, Wei Dong, Richard Socher, Li-Jia Li, Kai Li, and Li Fei-Fei. Imagenet: A large-scale hierarchical image database. In *IEEE Conference on Computer Vision and Pattern Recognition (CVPR)*, pages 248–255. Ieee, 2009. [5](#), [11](#)
- [8] Jonas Geiping, Micah Goldblum, Phillip E Pope, Michael Moeller, and Tom Goldstein. Stochastic training is not necessary for generalization. *arXiv preprint arXiv:2109.14119*, 2021. [2](#)
- [9] Ian J Goodfellow, Jonathon Shlens, and Christian Szegedy. Explaining and harnessing adversarial examples. In *International Conference on Learning Representations (ICLR)*, 2015. [1](#)
- [10] Frithjof Gressmann, Zach Eaton-Rosen, and Carlo Luschi. Improving neural network training in low dimensional random bases. In *Advances in Neural Information Processing Systems (NeurIPS)*, volume 33, pages 12140–12150, 2020. [3](#)
- [11] Guy Gur-Ari, Daniel A Roberts, and Ethan Dyer. Gradient descent happens in a tiny subspace. *arXiv preprint arXiv:1812.04754*, 2018. [3](#)
- [12] Kaiming He, Xiangyu Zhang, Shaoqing Ren, and Jian Sun. Deep residual learning for image recognition. In *the IEEE/CVF Conference on Computer Vision and Pattern Recognition (CVPR)*, pages 770–778, 2016. [5](#), [11](#)
- [13] Yiding Jiang, Behnam Neyshabur, Hossein Mobahi, Dilip Krishnan, and Samy Bengio. Fantastic generalization measures and where to find them. In *International Conference on Learning Representations (ICLR)*, 2020. [2](#)
- [14] Hoki Kim, Woojin Lee, and Jaewook Lee. Understanding catastrophic overfitting in single-step adversarial training. In *AAAI*, pages 8119–8127, 2020. [1](#), [2](#), [3](#), [6](#)
- [15] Alex Krizhevsky, Geoffrey Hinton, et al. Learning multiple layers of features from tiny images. *Technical Report*, 2009. [5](#)
- [16] Chunyuan Li, Heerad Farkhoor, Rosanne Liu, and Jason Yosinski. Measuring the intrinsic dimension of objective landscapes. In *International Conference on Learning Representations (ICLR)*, 2018. [3](#)
- [17] Tao Li, Lei Tan, Qinghua Tao, Yipeng Liu, and Xiaolin Huang. Low dimensional landscape hypothesis is true: DNNs can be trained in tiny subspaces. *arXiv preprint arXiv:2103.11154*, 2021. [2](#), [3](#), [4](#), [8](#), [11](#)
- [18] Fangzhou Liao, Ming Liang, Yinpeng Dong, Tianyu Pang, Xiaolin Hu, and Jun Zhu. Defense against adversarial attacks using high-level representation guided denoiser. In *the IEEE/CVF Conference on Computer Vision and Pattern Recognition (CVPR)*, 2018. [3](#)
- [19] Aleksander Madry, Aleksandar Makelov, Ludwig Schmidt, Dimitris Tsipras, and Adrian Vladu. Towards deep learning models resistant to adversarial attacks. In *International Conference on Learning Representations (ICLR)*, 2018. [1](#), [3](#), [7](#)
- [20] Seyed-Mohsen Moosavi-Dezfooli, Alhussein Fawzi, Jonathan Uesato, and Pascal Frossard. Robustness via curvature regularization, and vice versa. In *Proceedings of the IEEE/CVF Conference on Computer Vision and Pattern Recognition (CVPR)*, pages 9078–9086, 2019. [3](#)
- [21] Nicolas Papernot, Patrick McDaniel, Ian Goodfellow, Somesh Jha, Z Berkay Celik, and Ananthram Swami. Practical black-box attacks against machine learning. In *Proceedings of the 2017 ACM on Asia Conference on Computer and Communications Security*, pages 506–519, 2017. [8](#), [11](#)
- [22] Nicolas Papernot, Patrick McDaniel, Xi Wu, Somesh Jha, and Ananthram Swami. Distillation as a defense to adversarial perturbations against deep neural networks. In *2016 IEEE symposium on security and privacy (SP)*, pages 582–597. IEEE, 2016. [3](#)
- [23] Leslie Rice, Eric Wong, and Zico Kolter. Overfitting in adversarially robust deep learning. In *International Conference on Machine Learning (ICML)*, pages 8093–8104. PMLR, 2020. [2](#), [3](#), [5](#), [6](#)
- [24] Ali Shafahi, Mahyar Najibi, Mohammad Amin Ghiasi, Zheng Xu, John Dickerson, Christoph Studer, Larry S. Davis, Gavin Taylor, and Tom Goldstein. Adversarial training for free. In *Advances in Neural Information Processing Systems (NeurIPS)*, volume 32, pages 3353–3364, 2019. [3](#), [6](#)
- [25] Florian Tramèr, Alexey Kurakin, Nicolas Papernot, Ian J. Goodfellow, Dan Boneh, and Patrick D. McDaniel. Ensemble adversarial training: Attacks and defenses. In *6th International Conference on Learning Representations (ICLR)*, 2018. [3](#)
- [26] Mark Tuddenham, Adam Prügél-Bennett, and Jonathan Hare. Quasi-newton’s method in the class gradient defined high-curvature subspace. *arXiv preprint arXiv:2012.01938*, 2020. [3](#)

- [27] BS Vivek and R Venkatesh Babu. Single-step adversarial training with dropout scheduling. In *2020 IEEE/CVF Conference on Computer Vision and Pattern Recognition (CVPR)*, pages 947–956. IEEE, 2020. 3
- [28] Yisen Wang, Difan Zou, Jinfeng Yi, James Bailey, Xingjun Ma, and Quanquan Gu. Improving adversarial robustness requires revisiting misclassified examples. In *International Conference on Learning Representations (ICLR)*, 2019. 3
- [29] Eric Wong and Zico Kolter. Provable defenses against adversarial examples via the convex outer adversarial polytope. In *International Conference on Machine Learning (ICML)*, pages 5286–5295. PMLR, 2018. 3
- [30] Eric Wong, Leslie Rice, and J. Zico Kolter. Fast is better than free: Revisiting adversarial training. In *International Conference on Learning Representations (ICLR)*, 2020. 1, 2, 3, 4, 5, 6, 7
- [31] Sergey Zagoruyko and Nikos Komodakis. Wide residual networks. In *British Machine Vision Conference (BMVC)*, 2016. 5, 12
- [32] Valentina Zantedeschi, Maria-Irina Nicolae, and Amrith Rawat. Efficient defenses against adversarial attacks. In *Proceedings of the 10th ACM Workshop on Artificial Intelligence and Security*, pages 39–49, 2017. 3
- [33] Hongyang Zhang, Yaodong Yu, Jiantao Jiao, Eric P. Xing, Laurent El Ghaoui, and Michael I. Jordan. Theoretically principled trade-off between robustness and accuracy. In *International Conference on Machine Learning (ICML)*, pages 7472–7482, 2019. 3

## Supplementary Material for Subspace Adversarial Training

### A. Detailed Sampling Strategy

We present a detailed sampling strategy of model checkpoints for DLDR [17] in Tab. A2, where we consider the times of uniform sampling in each epoch, the number of sampling epochs, the total number of samplings, and the dimension of the subspace extracted from the samplings. The general sampling strategy is quite simple: we uniformly sample a few checkpoints in every training epoch before the overfitting occurs. For single-step AT, the exact time when catastrophic overfitting occurs may be slightly different for different runs. Our sampling strategy is a conservative and robust one. We suggest sampling as more as model checkpoints before the overfitting occurs to estimate the subspace more accurately and achieve better results. Note that the total number of samplings  $t$  is actually small (around 200), and thus the computational overhead on the corresponding decomposition of a  $t \times t$  matrix is small. This explains why the computational cost of the decomposition is negligible compared to the total computational cost. A more delicate sampling strategy design may improve the performance and could be an interesting topic for future works.

**Ablation study for the dimension  $d$ .** We provide an ablation study for the dimension of the subspace  $d$  in Fig. A1, where we vary the dimension of the subspace for Fast Sub-AT from 50 to 100 and record the best robust accuracy obtained in corresponding subspaces. We observe that the best robust accuracy varies very little across such a wide range of dimensions (<1%). Thus we conclude that our Sub-AT is robust to the exact choice of the dimension  $d$ .

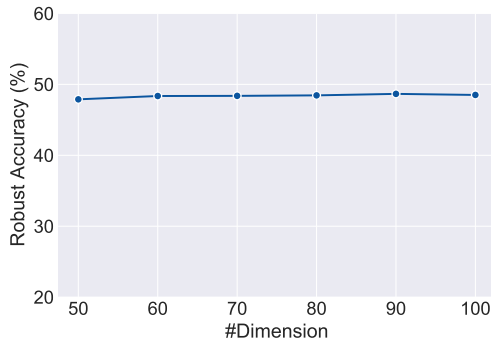


Figure A1. Ablation study for the dimension of the subspace  $d$  on CIFAR-10. Fast Sub-AT can achieve similar best robustness performance across a wide range of dimensions. The robust accuracy is evaluated under PGD-20 attack.

### B. Additional Results under Auto-Attack

We further evaluate the performance of Sub-AT on mitigating robust overfitting in multi-step AT with Auto-Attack, a stronger and more reliable attack proposed by Croce *et al.* [6]. From the results in Tab. A1, we observe that our Sub-AT can indeed effectively mitigate the robust overfitting and then consistently improve the robust accuracy. Hence, training in subspace can genuinely overcome the overfitting and improve the model robustness rather than as a result of gradient masking [2,21].

Table A1. Robust accuracy of multi-step AT and Sub-AT on CIFAR-10/100 against  $\ell_2$  and  $\ell_\infty$  adversarial perturbations. The robust accuracy is evaluated under Auto-Attack [6]. Our Sub-AT can achieve consistent improvements on the robust accuracy while effectively mitigating the robust overfitting. The best robustness performances and the smallest difference between the best and the final are marked in **bold**.

| Dataset   | Norm          | Settings | Auto-Attack  |              |              |
|-----------|---------------|----------|--------------|--------------|--------------|
|           |               |          | Best         | Final        | Diff.        |
| CIFAR-10  | $\ell_\infty$ | AT       | 47.29        | 41.08        | 6.21         |
|           |               | Sub-AT   | <b>48.37</b> | <b>47.88</b> | <b>0.49</b>  |
|           | $\ell_2$      | AT       | 65.66        | 63.93        | 1.73         |
|           |               | Sub-AT   | <b>66.99</b> | <b>67.15</b> | <b>-0.16</b> |
| CIFAR-100 | $\ell_\infty$ | AT       | 22.83        | 18.12        | 4.71         |
|           |               | Sub-AT   | <b>23.89</b> | <b>23.83</b> | <b>0.06</b>  |
|           | $\ell_2$      | AT       | 36.91        | 32.70        | 4.21         |
|           |               | Sub-AT   | <b>38.14</b> | <b>37.84</b> | <b>0.30</b>  |

### C. Results on Tiny-ImageNet

We report the results on Tiny-ImageNet [7] in Tab. A3, where we use PreAct ResNet18 model [12] as default and train the model for 100 epochs with learning rate decay at 50 and 80 following [4]. Sub-AT is trained for 20 epochs with a constant learning rate 1, accordingly. For single-step Fast AT, we observe that the catastrophic overfitting occurs at the 17th epoch, and thus we only sample for 16 epochs. Even with such few samplings, we can obtain an 18.79% robust accuracy with only a single-step gradient, while standard PGD-10 AT achieves a slightly better robust accuracy 19.84% with around **12x** training time overhead and, even worse, serious robust overfitting problem. Within the better subspace extracted from the PGD-10 AT, our Fast Sub-AT can achieve **21.87%** robust accuracy, which is significantly better than the PGD-10 AT and also enjoys great computational benefits.

Table A2. Detailed sampling strategy for DLDR. We report the times of uniformly sampling in each epoch of training, the number of sampling epochs, the total number of samplings  $t$ , and the dimension of the subspace extracted from the samplings of parameters. Note that there is an additional sampling on the parameter initialization as we start the Sub-AT from the initialization.

| Type        | Datasets      | Method    | #Times/epoch | #Epochs | $t$ | #Dimension |
|-------------|---------------|-----------|--------------|---------|-----|------------|
| Single-step | CIFAR-10      | Fast AT   | 2            | 65      | 131 | 80         |
|             | CIFAR-10      | GradAlign | 2            | 65      | 131 | 100        |
|             | CIFAR-100     | Fast AT   | 2            | 65      | 131 | 80         |
|             | CIFAR-100     | GradAlign | 2            | 65      | 131 | 100        |
|             | Tiny-ImageNet | Fast AT   | 4            | 16      | 65  | 50         |
| Multi-step  | CIFAR-10      | PGD-10 AT | 2            | 100     | 201 | 120        |
|             | CIFAR-100     | PGD-10 AT | 2            | 100     | 201 | 120        |
|             | Tiny-ImageNet | PGD-10 AT | 4            | 50      | 201 | 120        |

Table A3. Results on Tiny-ImageNet. We use PreAct ResNet18 model and consider both single-step AT and multi-step AT. The time consumption is evaluated on an Nvidia Tesla V100. Sub-AT demonstrates its superior performance in both robustness performance and computational overhead.

| Method             | Subspace                            | Best      |        | Final        |        | Time         |       |
|--------------------|-------------------------------------|-----------|--------|--------------|--------|--------------|-------|
|                    |                                     | Natural   | PGD-20 | Natural      | PGD-20 |              |       |
| <b>Single-step</b> | Fast AT                             | –         | 28.79  | 11.90        | 42.54  | 0.00         | 3.5h  |
|                    | Fast Sub-AT ( $\epsilon = 8/255$ )  | Fast AT   | 39.38  | 16.75        | 39.19  | 16.17        | 1.3h  |
|                    | Fast Sub-AT ( $\epsilon = 12/255$ ) | Fast AT   | 38.11  | 18.52        | 38.306 | 18.13        | 1.3h  |
|                    | Fast Sub-AT ( $\epsilon = 16/255$ ) | Fast AT   | 37.32  | <b>18.79</b> | 37.20  | <b>18.22</b> | 1.3h  |
| <b>Multi-step</b>  | PGD-10 AT                           | –         | 42.76  | 19.84        | 46.57  | 14.18        | 15.7h |
|                    | PGD-10 Sub-AT                       | PGD-10 AT | 40.82  | 20.52        | 40.78  | 19.55        | 12.1h |
|                    | PGD-10 AT ( $\epsilon = 12/255$ )   | PGD-10 AT | 40.88  | 21.42        | 42.27  | 21.41        | 8.6h  |
|                    | PGD-10 AT ( $\epsilon = 16/255$ )   | PGD-10 AT | 40.99  | <b>21.87</b> | 41.27  | <b>21.60</b> | 8.6h  |

Table A4. Results on multi-step PGD-10 AT and Sub-AT with WideResNet-28-10 model against **PGD-20** attack with  $\ell_\infty$  perturbations with radius  $8/255$ .

| Dataset   | Settings | Robust Accuracy |              |             | Natural Accuracy |       |       |
|-----------|----------|-----------------|--------------|-------------|------------------|-------|-------|
|           |          | Best            | Final        | Diff.       | Best             | Final | Diff. |
| CIFAR-10  | AT       | 53.26           | 46.70        | 6.56        | 84.69            | 85.81 | -1.12 |
|           | Sub-AT   | <b>55.14</b>    | <b>54.75</b> | <b>0.39</b> | 84.79            | 84.71 | 0.08  |
| CIFAR-100 | AT       | 29.44           | 23.26        | 6.18        | 57.64            | 56.08 | 1.56  |
|           | Sub-AT   | <b>31.07</b>    | <b>30.69</b> | <b>0.38</b> | 57.24            | 57.40 | -0.16 |

## D. Results on Wide-ResNet

We conduct further experiments on Wide-ResNet [31] architectures. Specifically, we use the WideResNet-28-10 model and consider  $\ell_\infty$  adversarial perturbations with radius  $8/255$  on CIFAR-10 and CIFAR-100. From the results in Tab. A4, we observe that similarly, the robust overfitting can be successfully mitigated meanwhile with significant improvements in robustness. We achieve **+1.88%** on CIFAR-10 and **+1.63%** on CIFAR-100 and successfully control the robust accuracy gap between the best and the fi-

nal under 0.4%. Thus we conclude that our Sub-AT can also be easily applied to other commonly used architectures and obtain similar enhancements in robustness.